Batteries & Supercaps

Research Article
doi.org/10.1002/batt.202300170

Chemistry Europe
European Chemical Societies Publishing

www.batteries-supercaps.org

VIP *Very Important Paper*

Special Collection

Mitigation of Binder Migration Behavior during the Drying Process by Applying an Electric Field for Fast-Charging in Lithium-Ion Batteries

Keemin Park,[a] Myeungwoo Ryu,[a] Yongmin Jung,[a] Hee Eun Yoo,[a, b] Seungcheol Myeong,[a] Dongsoo Lee,[a] Soo Chan Kim,[c] Chanho Kim,[a] Jeongheon Kim,[a] Jiseok Kwon,[a] Kangchun Lee,[a] Chae-Woong Cho,*[d] Ungyu Paik,*[a] and Taeseup Song*[a, e]

The binder migration due to the capillary force-driven solvent evaporation during the drying process in the electrode manufacturing process induces inhomogeneous binder distribution in the electrode, which deteriorates Li-ion kinetics and corresponding poor fast-charging properties in lithium-ion batteries (LIBs). Here, we report an effective strategy to mitigate the binder migration behavior by applying an electric field during the drying process. As the employed carboxymethyl cellulose (CMC) and styrene-butadiene rubber (SBR) binders have a negative charge in an aqueous anode slurry system (pH 7), the binder migration behavior could be mitigated by generating an electrical attraction force into the bottom direction by positive electrification of the current collector. The anode prepared with electric field exhibits homogeneous binder distribution in the longitudinal direction, which enhances Li-ion kinetics, corresponding constant current charging capacity, and cycling stability compared to those of the anode prepared without electric field.

Introduction

Lithium-ion batteries (LIBs) with high energy density and fast-charging properties are demanded along with the rapid development of electric vehicles and energy storage systems.[1] Research on high performance LIBs has mainly focused on high-capacity active materials, and the significance of polymeric binders has been underestimated due to their low contents in the electrode and their electrochemically non-reactive properties during cell operation.[2] However, binders are indispensable additives that enable stable cell operation by maintaining the active materials together (cohesion) and bonding the electrode film to the current collector (adhesion).[3] Accordingly, the binder distribution in the electrode can significantly affect the electrochemical performances of the LIBs.[4]

The binders migrate to the electrode surface due to the capillary force-driven solvent evaporation during the drying process in the electrode manufacturing process, which causes inhomogeneous binder distribution in the electrode through the longitudinal direction.[4b,5] Adhesion strength between the electrode film and the current collector is deteriorated due to the small amount of binder near the interface between the electrode film and the current collector.[6] Furthermore, a large amount of binder on the electrode surface degrades Li-ion kinetics due to the tortuosity increase and corresponding electrochemical performances of LIBs by limiting electrolyte transport through the pores in the electrode.[4b,7] As the electrode becomes thicker to enhance the energy density of LIBs, the binder migration behavior is accelerated due to the longer drying time for complete solvent evaporation in the electrode, which deteriorates electrochemical performances of LIBs caused by the low adhesion strength and Li-ion kinetics.[8] Therefore, to realize high energy density LIBs, it is essential to improve the electrochemical performances of LIBs by controlling the binder migration behavior during the drying process.

Carboxymethyl cellulose (CMC) and styrene-butadiene rubber (SBR) have been widely used as aqueous binders.[9] The carboxymethyl group of CMC derived from the hydroxyl group on cellulose is dissociated into a carboxylate group, which presents a negative charge.[10] SBR is a synthetic rubber comprising styrene and butadiene units, which is insoluble in

[a] *K. Park, M. Ryu, Y. Jung, H. E. Yoo, S. Myeong, D. Lee, C. Kim, J. Kim, J. Kwon, K. Lee, Prof. U. Paik, Prof. T. Song*
Department of Energy Engineering
Hanyang University
222 Wangsimni-ro, 04763 Seoul (Republic of Korea)
E-mail: upaik@hanyang.ac.kr
tssong@hanyang.ac.kr

[b] *H. E. Yoo*
SB) Pouch Development Team
Samsung SDI
467 Beonyeong-ro, 31086 Cheonan (Republic of Korea)

[c] *S. C. Kim*
Lab) Electrode Development Group
Samsung SDI
130 Samsung-ro, 16678 Suwon (Republic of Korea)

[d] *C.-W. Cho*
GPE) Process Development Team
Samsung SDI
150 Gongse-ro, 17084 Giheung (Republic of Korea)
E-mail: cw97.cho@samsung.com

[e] *Prof. T. Song*
Department of Battery Engineering
Hanyang University
222 Wangsimni-ro, 04763 Seoul (Republic of Korea)

Supporting information for this article is available on the WWW under https://doi.org/10.1002/batt.202300170

Special Collection *An invited contribution to a Special Collection on Young Scientists in Battery Research*

Research Article
doi.org/10.1002/batt.202300170
Chemistry Europe
European Chemical Societies Publishing

aqueous medium due to its hydrophobic properties.[11] Sodium dodecyl sulfate (SDS), widely known as anionic surfactant, is typically used to disperse SBR in water. SDS adsorbed on SBR exhibits a negative charge generating electrostatic repulsion force between SBR particles, which enables SBR to exist stably in water.[12]

Herein, we report an effective strategy to mitigate the binder migration behavior of the anode for improved electrochemical performances of LIBs. As the employed CMC and SBR binders have a negative charge in an aqueous anode slurry system (pH 7), the binder migration behavior associated with solvent evaporation could be mitigated by generating an electrical attraction force into the bottom direction with positive electrification of the current collector via applying an electric field during the drying process (Scheme 1). The electrical attraction force on binders into the bottom direction against the capillary force-driven solvent evaporation during the drying process enables homogeneous distribution of the binders, which results in the improvement in the adhesion strength between the electrode film and the Cu current collector and Li-ion kinetics caused by the reduced tortuosity. The anode prepared with electric field showed a higher constant current charging capacity (75.1 mAh g^{-1} at 2.0 C) compared to the anode prepared without electric field (64.8 mAh g^{-1} at 2.0 C). Furthermore, the anode prepared with electric field exhibited superior cycling performances (77.4% capacity retention after 100 cycles) compared to that of the anode prepared without electric field (66.4% capacity retention after 100 cycles) at a high current density of 2.0 C.

Results and Discussion

Anode properties prepared without and with electric field

The adhesion strength between the anode film and Cu current collector was measured using a 180° peel test for the anodes prepared with different applied voltages during the drying process.[13] As the less binder migration occurs, the greater the adhesion strength. The 180° peel test is a method that can indirectly indicate the binder distribution in the electrode.[4a] The adhesion strength was improved with the increased applied voltage and saturated at the applied voltage of 15 kV (Figure 1a). Based on the adhesion strength results, the applied voltage generating an electric field for mitigating the binder migration behavior was set to 15 kV. The magnitude of applied electric field (E) could be calculated as follows;

$$E = \frac{V}{d}$$

Here, V is the applied voltage (V), and d is distance between the two electrodes (m). As the applied voltage to generate the electric field during the drying process is 15 kV, and the distance between the two electrodes is 15 cm, the magnitude of applied electric field is 10^5 V m^{-1}. In this case, the applied electric field is perpendicular to the Cu current collector and directed from the bottom (interface between the anode film and the Cu current collector) to the top (interface between the anode and the electrolyte) position of the electrode. To analyze

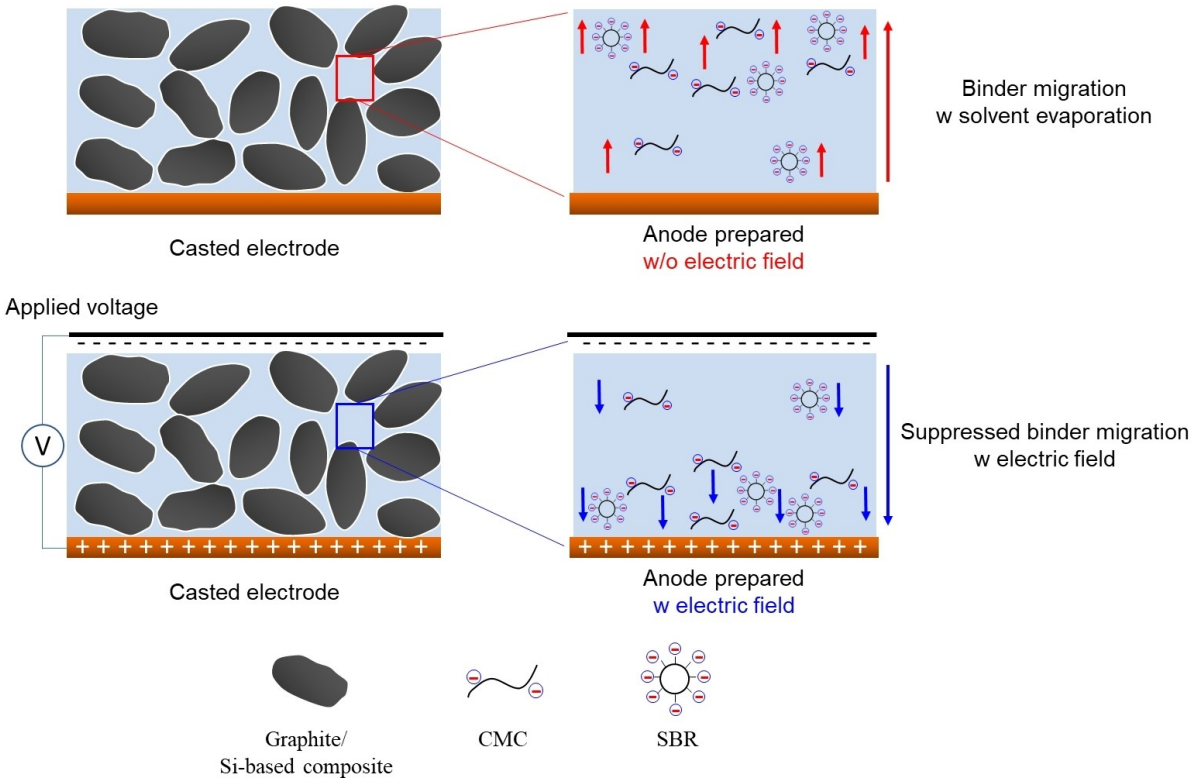

Scheme 1. Schematic illustration of the anode configurations during the drying process w/o (without) and with (w) electric field.

Research Article
doi.org/10.1002/batt.202300170
Chemistry Europe
European Chemical Societies Publishing

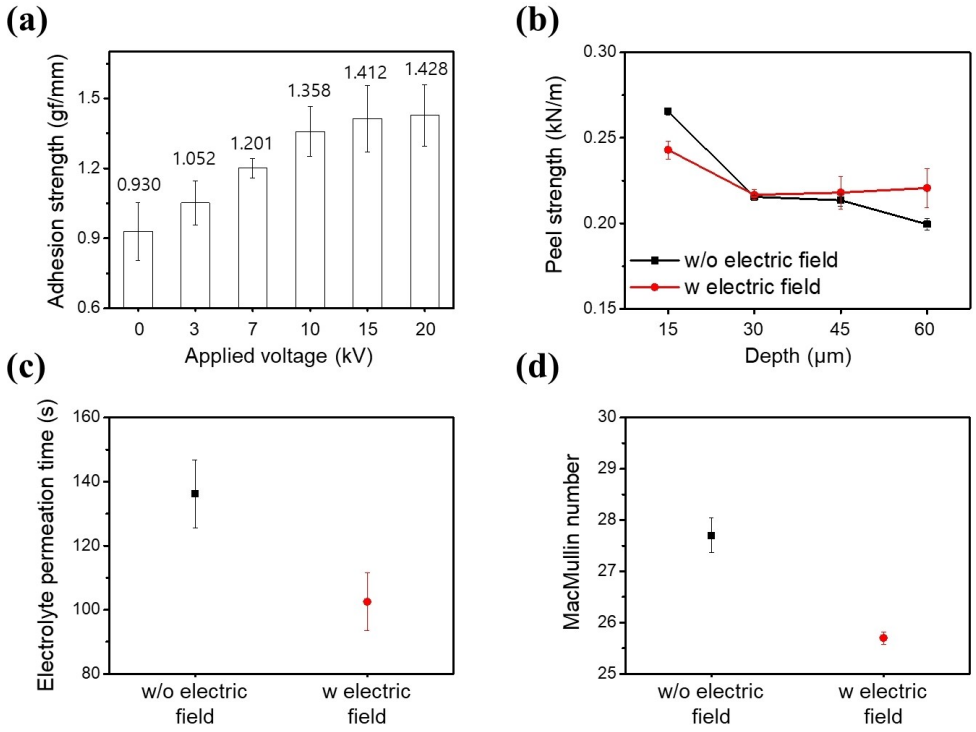

Figure 1. a) Adhesion strength of the anode with different applied voltages. b) Depth profiles of the peel strength depending on the anode w/o and with electric field. c) Electrolyte permeation time required for the electrolyte to completely penetrate the anode. d) MacMullin number (N_M) of the anodes.

the binder distribution in the longitudinal direction of the anodes prepared without (w/o) and with (w) electric field, the peel strength was obtained by scratching the inner layers from the surface of the anode every 15 μm (Figure 1b).[14] For both anodes, the peel strength at the top layer exhibited the largest value due to the binder migration behavior toward the electrode surface during the drying process of the anode.[15] The peel strength in the middle and bottom layers of the anode w/o electric field decreased 20%–25% compared to the top layer, while in the case of anode w electric field only about a 10% decrease was observed (Figure 1b and Table 1). Analysis of the peel strength in the longitudinal direction of the anode exhibits the controlled binder migration behavior by applying an electric field during the drying process.

The electrolyte permeability is closely related to the binder and pore distribution in the anode, which plays an important role in the electrochemical properties.[13,16] The binder on the surface of the anode can limit the electrolyte transport through the pores deteriorating the Li-ion kinetics of the anode and corresponding electrochemical performances of LIBs.[4b,7] The anode w electric field exhibits a better electrolyte permeation of 102.5 s than the pristine anode of 136.2 s, which is attributed to the mitigation of the binder migration behavior during the drying process (Figure 1c). Similarly, the anode w electric field showed a smaller contact angle with the electrolyte than the pristine anode indicating better affinity with the electrolyte (Figure S1). Electrochemical impedance spectroscopy (EIS) analysis of the anode symmetric cells was conducted to explain the electrolyte transport through the pores in the anode.[17] The anode w electric field presented a lower ionic resistance (R_{ion}) of 15.9 Ω compared to that of the anode w/o electric field (17.1 Ω) (Figure S2). To elucidate the electrolyte transport in the anode regardless of the anode thickness, the MacMullin number (N_M) was obtained as follows;[18]

$$N_M = \frac{R_{ion} \cdot A \cdot \sigma_0}{d} \quad (1)$$

where R_{ion} is the ionic resistance of the anode (Ω), A is the electrode area (cm^2), σ_o is the ionic conductivity of the electrolyte ($S\,cm^{-1}$), and d is the electrode thickness (μm). The values of the parameters required to calculate the N_M of the anode w/o and with electric field are listed in Table S1. As shown in Figure 1(d), the N_M of the anode w/o electric field was 27.7. In comparison, the anode with electric field had a lower value of N_M (25.7). This result agrees well with the electrolyte perme-

Table 1. Peel strength and retention dependent on the longitudinal depth profiles in anodes prepared w/o and w electric field displayed in Figure 1(b).

Layer	Vertical depth [μm]	w/o electric field		w electric field	
		Peel strength [kN/m]	Strength retention [%]	Peel strength [kN/m]	Strength retention [%]
Top	15	0.2655	100	0.2430	100
Middle	30	0.2155	81.2	0.2167	89.2
	45	0.2135	80.4	0.2180	89.7
Bottom	60	0.1995	75.1	0.2207	90.8

Research Article
doi.org/10.1002/batt.202300170
Chemistry Europe
European Chemical Societies Publishing

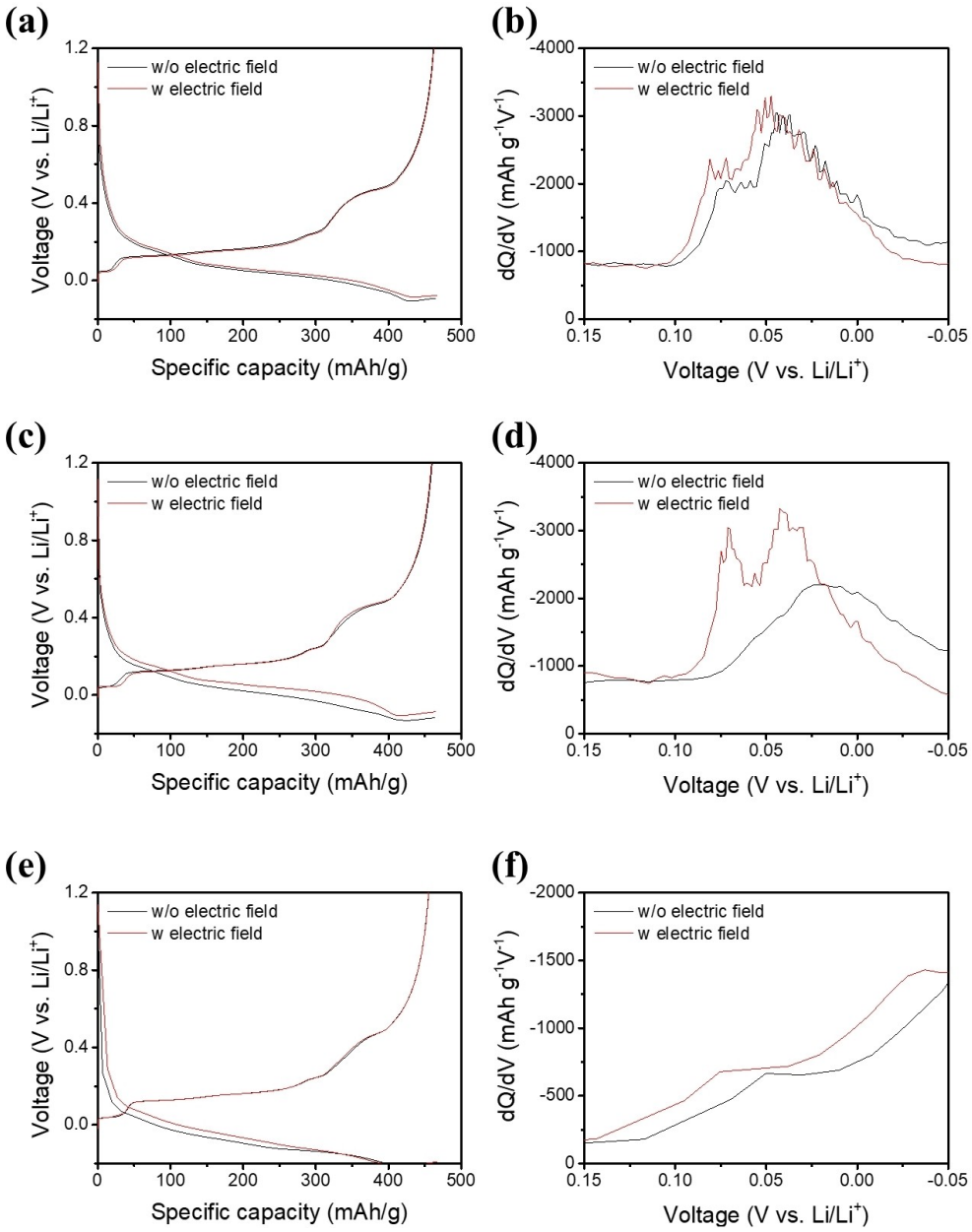

Figure 2. Voltage profiles of the anodes half-cells prepared w/o and with electric field at a) 0.5 C, c) 1.0 C, and e) 2.0 C discharging (lithiation) rates after the formation cycle. The charging (delithiation) rate was maintained at 0.2 C. b), d), and f) Differential capacity vs. voltage (d*Q*/d*V* vs. *V*) curves for anodes w/o and with electric field derived from the discharging curves of (a), (c), and (e), respectively.

ability test, which means that Li-ion kinetics was improved by mitigating the binder migration behavior via applying an electric field during the drying process.

Electrochemical properties

The electrochemical properties of the anodes prepared w/o and w electric field were evaluated to prove the effect of enhanced Li-ion kinetics associated with binder migration control. Figure S3 shows the voltage profiles of the anodes prepared w/o and w electric field at the first 0.1 C cycle in the voltage range of 0.01–1.2 V vs. Li/Li^+. The charging (delithiation) capacity of the anode w/o electric field was 438.9 mAh g^{-1}, and a coulombic efficiency was 88.7%, which is nearly the same as that of the anode w electric field (charging capacity of 436.5 mAh g^{-1} and coulombic efficiency of 88.6%). To analyze the discharging (lithiation) properties depending on the application of an electric field, the voltage profiles were presented by increasing the discharging C-rate to 0.5, 1.0, and 2.0. At the same time, the charging C-rate was fixed at 0.2 C. The end condition of discharging patterns in the half-cell was set as a voltage range of −0.5 V and as an areal capacity of 5.5 mAh cm^{-2}. As the discharging rate increased from 0.5 C to

Research Article
doi.org/10.1002/batt.202300170
Chemistry Europe
European Chemical Societies Publishing

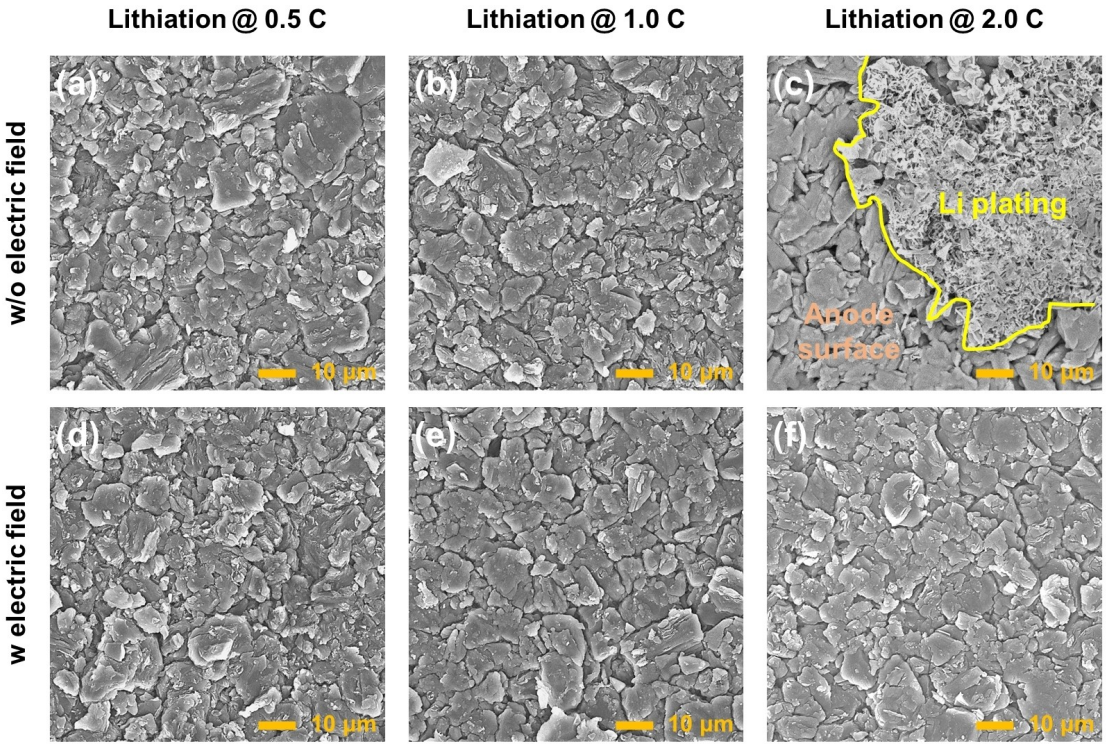

Figure 3. SEM images of the anode surface depending on discharging C-rate of 0.5, 1.0, and 2.0 after the formation cycles: a–c) anode w/o electric field and d–f) anode with electric field.

1.0 and 2.0 C, the lithiation overpotentials increased in both anodes (Figure 2a, c and e). However, the overpotentials were relatively small in the anode w electric field compared to those of the anode w/o electric field, which is attributed to the enhanced Li-ion kinetics.[19] Figure 2(b) shows the differential capacity versus voltage curve for the anode w/o and with electric field at a discharging rate of 0.5 C. The two main peaks of the anodes are related to the Li-ion intercalation into the graphite material during the lithiation.[20] In the anode with electric field, compared to the w/o electric field, the peak intensity is significant, and the overpotential is small, which indicates facile intercalation of Li-ions into the graphite material.[21] At a discharging rate of 1.0 C, the anode with electric field clearly showed two peaks of Li-ion intercalation into the graphite material. In contrast, the anode w/o electric field exhibited only one peak related to the Li-ion intercalation due to the large overpotential during discharging associated with low Li-ion kinetics (Figure 2d).[22] As shown in Figure 2(f), the Li-ion intercalation peak into the graphite material was not observed in both anodes at a large current density of 2.0 C; however, the discharging overpotential of the anode w electric field was still small compared to that of the anode w/o electric field. The redox reaction during lithiation/delithiation process was analyzed by cyclic voltammetry (CV) test for anodes w/o and w electric field.[23] To accurately investigate the redox reaction of the active materials with Li-ions, focusing specifically on the reaction between the active materials and the Li-ions rather than the formation of the solid electrolyte interphase (SEI) layer, the CV measurement of the 2nd cycle was obtained following the initial formation cycle. As shown in Figure S4, both anodes exhibited lithiation peaks below 0.3 V and delithiation peaks at 0.2–0.3 V, showing CV curves of a typical graphite-based anode.[24] And anode w electric field presented a larger peak current compared to that of the anode w/o electric field, which means better redox reactivity with Li-ion.[25] To investigate the diffusion coefficient of Li-ion (D_{Li+}) for anodes w/o and w electric field, Galvanostatic Intermittent Titration Technique (GITT) experiments were performed on the half-cell during discharge (lithiation) process at 0.1 C, respectively (Figure S5). The diffusion coefficient of Li-ion could be calculated as follows;[26]

$$D_{Li^+} = \frac{4}{\pi\tau}\left(\frac{m_B V_m}{M_B A}\right)^2 \left(\frac{\Delta E_s}{\Delta E_t}\right)^2 \quad (2)$$

here τ is the constant current pulse duration (s), m_B is the weight of the active material (g), V_m is the molar volume of the active material ($cm^3\,mol^{-1}$), M_B is the molecular weight of the active material ($g\,mol^{-1}$), A is the contact area between the electrode-electrolyte interface (cm^2), ΔE_s is the change of the potential in the steady-state during the single-step GITT test (V), and ΔE_t is the total change in potentials during the constant current pulse duration of the sing-step GITT test (V). As shown in Figure S6, the anode with electric field showed higher D_{Li+} at all potentials during lithiation process compared to anode w/o electric field. These results exhibit that the Li-ion transport behavior was improved by inducing uniform longitudinal binder distribution in the anode via applying electric field during the drying process.

Research Article
doi.org/10.1002/batt.202300170
Chemistry Europe
European Chemical Societies Publishing

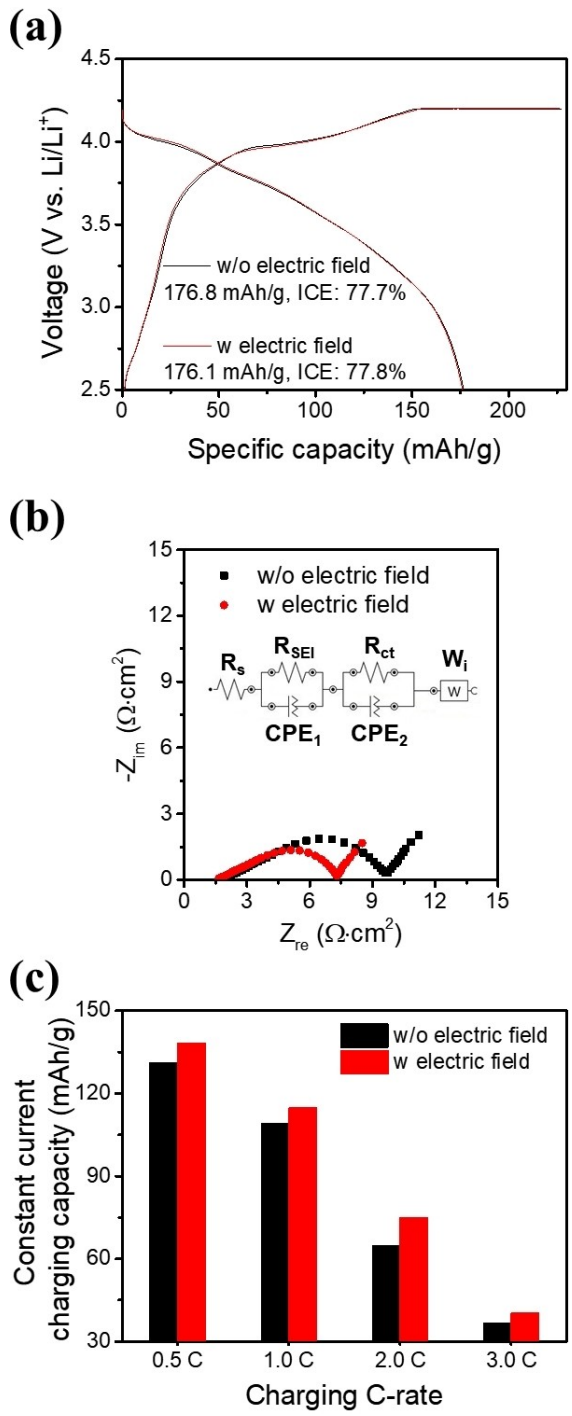

Figure 4. a) Initial charge/discharge voltage profile of the full-cells comprising an NCA cathode and anodes prepared w/o and w electric field at 0.1 C. b) Nyquist plot of the full-cells after 0.1 and 0.2 C formation cycles. c) Constant current charging capacity of the full-cells depending on the charging C-rate.

Figure 3 shows the SEM images of an anode surface prepared w/o and with electric field depending on the discharging (lithiation) C-rate of 0.5, 1.0, and 2.0 after the formation cycles in the half-cell test. For the anode w/o electric field, Li plating was not observed on the anode surface during the discharging process at 0.5 and 1.0 C; however, Li plating occurred on the anode surface at 2.0 C (Figure 3a–c). This is attributed to the large overpotentials during the 2.0 C discharging process associated with poor Li-ion kinetics of the anode w/o electric field.[27] In the anode w electric field, Li plating did not appear in all discharging C-rate of 0.5, 1.0, and 2.0 due to the improved Li-ion kinetics with homogeneous binder distribution in the anode by applying electric field during the drying process, which presents the superior discharging (lithiation) properties at a high C-rate (Figure 3d–f). The crystalline structure of the anode w/o electric field lithiated at 2.0 C was analyzed through X-ray diffraction (XRD). The lithiated anode mainly shows LiC_{30} phase, which means that Li was not completely intercalated into the graphite at 2.0 C (Figure S7).[28] In addition, there is a Li metal peak around 36°, indicating that Li metal of (110) plane is precipitated on the graphite surface.[29] The surface chemistry of the precipitated Li metal was analyzed by X-ray photoelectron spectroscopy (XPS). The deconvoluted peak of Li 1s exhibits the Li and Li compounds of LiF and Li_2O formed by the reaction between the Li and the electrolyte (Figure S8).[30] The anode with an areal capacity of 5.5 mAh cm^{-2} was prepared for the coin full-cell test using $LiNi_{0.8}Co_{0.15}Al_{0.05}O_2$ (NCA) with an areal capacity of 5 mAh cm^{-2} as the cathode. Figure 4(a) shows the initial charge/discharge voltage profiles of the full-cells at a 0.1 C rate. Similar to the half-cell results, there was no noticeable difference between the two full-cells comprising NCA and the anode w/o and with electric field due to the low current density of 0.1 and 0.2 C (Figures 4a and S9). Figure 4(b) shows the Nyquist plot of the full-cells after the two-step formation cycles at 0.1 and 0.2 C. The anode w electric field exhibited lower resistance of solution (R_s, high-frequency resistance), a solid-electrolyte interphase (SEI) layer (R_{SEI}, the 1st semi-circle in high-frequency range), and charge transfer (R_{ct}, the 2nd in medium frequency range) compared with those of the anode w/o electric field (Figure 4b and Table 2).[31] The quick-charging test of the full-cells was evaluated up to a charging rate of 3.0 C, maintaining the discharging rate at 0.5 C, as shown in Figure S10. The anodes w/o and with electric field presented no noticeable difference in the capacity retention in the whole C-rate due to the cells charged in the constant current and constant voltage (CC–CV) condition. However, when the charging capacity was considered only as a constant current (CC) region, the anode w electric field showed high charging capacities up to 3.0 C compared to those of the anode w/o electric field (Figures 4c and S11).[32] The above results demonstrate that quick charging properties can be improved by employing an anode w electric field due to the enhanced Li-ion kinetics.[33]

To evaluate the cycling performance, the anodes w/o and with electric field were tested at 1.0 C for 70 cycles, as shown in Figure 5(a). After the 0.1 and 0.2 C formation cycles, the cell

Table 2. Kinetic factors of the anodes w/o and w electric field in full-cells.

	R_s [Ω·cm^2]	R_{SEI} [Ω·cm^2]	R_{ct} [Ω·cm^2]
w/o electric field	2.001	2.974	4.816
w electric field	1.641	2.101	3.039

Research Article
doi.org/10.1002/batt.202300170
Chemistry Europe
European Chemical Societies Publishing

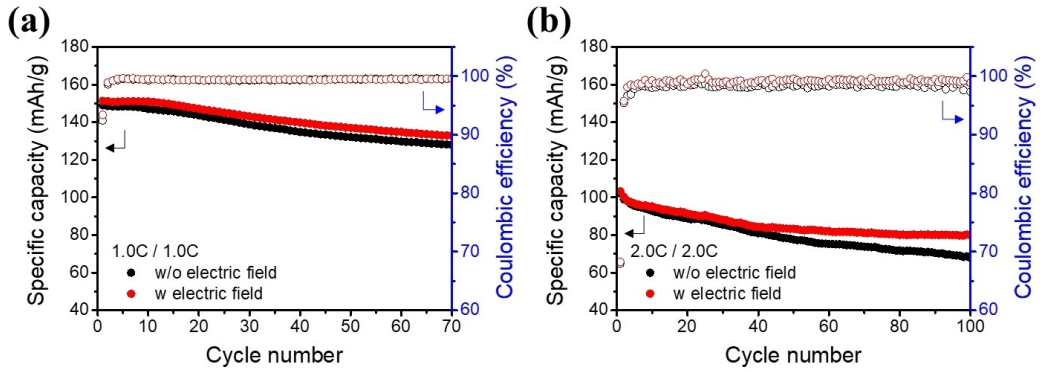

Figure 5. Cycling stabilities of the full-cells comprising an NCA cathode and anodes prepared w/o and w electric field at a) 1.0 C and b) 2.0 C.

comprising NCA and the anode w/o electric field exhibited capacity retention of 85.5% at 70 cycles. Similarly, the anode w electric field showed capacity retention of 87.7% at 70 cycles. The anodes w/o and w electric field were also evaluated at 2.0 C for 100 cycles after the formation cycles (Figure 5b). The anode w electric field exhibited capacity fading in earlier cycles, and the capacity retention was 81.7% at 40 cycles. However, the anode w electric field showed superior stable cycling properties after 40 cycles, indicating capacity retention of 77.4% over 100 cycles, which might be attributed to the released stress of the Si-based materials during the cycle test.[34] The anode w/o electric field presented continuous capacity fading and capacity retention of 79.4% at 40 cycles and 66.4% at 100 cycles. The electrochemical impedance spectroscopy (EIS) results revealed a lower R_{ct} in the anode w electric field than that of the anode w/o electric field after 100 cycles at 2.0 C (Figure S12).[35]

As R_{ct} is affected by R_{ion}, the low R_{ct} values of anode w electric field compared to those of the anode w/o electric field before and after cycle test could be attributed to the improved R_{ion} associated with homogeneous binder distribution by applied electric field during the drying process.[36] The results of polarization curve during Li-ion intercalation, fast-charging properties, and cycle retention clearly indicate that mitigation of the binder migration behavior by applying an electric field during the drying process plays an important role in the enhancement of Li-ion kinetics and electrochemical properties in LIBs.

Conclusions

The binder migration behavior in the anode was successfully mitigated by applying an electric field during the drying process. As employed CMC and SBR binders have a negative charge in an aqueous anode slurry system, the binder migration behavior could be alleviated by generating an electrical attraction force into the bottom direction by positive electrification of the current collector via applying an electric field during the drying process. The anode prepared with electric field shows homogeneous binder distribution in the longitudinal direction, which enhances Li-ion kinetics in the anode. As a result, the anode prepared with electric field exhibits improved Li-ion kinetics, reduced overpotential during the lithiation, and enhanced fast-charging properties and cycling stability compared to those of the pristine anode.

Experimental Section

All experimental details are included in the Supporting Information.

Supporting Information

Supporting Information is available from the Wiley Online Library or from the author.

Acknowledgements

This work was supported by the Human Resources Program in Energy Technology of the Korea Institute of Energy Technology Evaluation and Planning (KETEP), which was granted financial resources from the Ministry of Trade, Industry & Energy, Republic of Korea (No. 20214000000520). This work was also supported by the Ministry of Trade, Industry and Energy (MOTIE) of the Republic of Korea (No. 20009985).

Conflict of Interests

The authors declare no conflict of interest.

Data Availability Statement

The data that support the findings of this study are available in the supplementary material of this article.

Keywords: binder migration · lithium-ion batteries · drying process · electric field · fast-charging

[1] a) T. Song, J. L. Xia, J. H. Lee, D. H. Lee, M. S. Kwon, J. M. Choi, J. Wu, S. K. Doo, H. Chang, W. I. Park, D. S. Zang, H. Kim, Y. G. Huang, K. C. Hwang, J. A. Rogers, U. Paik, *Nano Lett.* **2010**, *10*, 1710–1716; b) D. Lee, A. Kondo, S. Lee, S. Myeong, S. Sun, I. Hwang, T. Song, M. Naito, U. Paik, *J. Power Sources* **2020**, *457*, 228021; c) Z. Li, Y. Zhang, T. Liu, X. Gao, S. Li, M. Ling, C. Liang, J. Zheng, Z. Lin, *Adv. Energy Mater.* **2020**, *10*, 1903110.

[2] a) H. Park, J. Kwon, H. Choi, D. Shin, T. Song, X. W. Lou, *ACS Nano* **2018**, *12*, 2827–2837; b) S. G. Patnaik, R. Vedarajan, N. Matsumi, *J. Mater. Chem. A* **2017**, *5*, 17909–17919.

[3] a) M. Muller, L. Pfaffmann, S. Jaiser, M. Baunach, V. Trouillet, F. Scheiba, P. Scharfer, W. Schabel, W. Bauer, *J. Power Sources* **2017**, *340*, 1–5; b) D. Qin, L. Xue, B. Du, J. Wang, F. Nie, L. Wen, *J. Mater. Chem. A* **2015**, *3*, 10928–10934.

[4] a) K. Kim, S. Byun, J. Choi, S. Hong, M. H. Ryou, Y. M. Lee, *ChemPhysChem* **2018**, *19*, 1627–1634; b) S. Jaiser, M. Muller, M. Baunach, W. Bauer, P. Scharfer, W. Schabel, *J. Power Sources* **2016**, *318*, 210–219; c) C. Jin, J. Nai, O. Sheng, H. Yuan, W. Zhang, X. Tao, X. W. Lou, *Energy Environ. Sci.* **2021**, *14*, 1326–1379.

[5] F. Font, B. Protas, G. Richardson, J. M. Foster, *J. Power Sources* **2018**, *393*, 177–185.

[6] J. Kumberg, M. Müller, R. Diehm, S. Spiegel, C. Wachsmann, W. Bauer, P. Scharfer, W. Schabel, *Energy Technol.* **2019**, *7*, 1900722.

[7] M. P. Lautenschlaeger, B. Prifling, B. Kellers, J. Weinmiller, T. Danner, V. Schmidt, A. Latz, *Batteries & Supercaps* **2022**, *5*, e202200090.

[8] a) B. G. Westphal, A. Kwade, *J. Energy Storage* **2018**, *18*, 509–517; b) K. Park, H. E. Yoo, Y. Jung, M. Ryu, S. Myeong, D. Lee, S. C. Kim, C. Kim, J. Kim, J. Kwon, K. Lee, C.-W. Cho, U. Paik, T. Song, *J. Power Sources* **2023**, *577*, 233238.

[9] a) J. H. Lee, U. Paik, V. A. Hackley, Y. M. Choi, *J. Electrochem. Soc.* **2005**, *152*, A1763–A1769; b) H. Buqa, M. Holzapfel, F. Krumeich, C. Veit, P. Novák, *J. Power Sources* **2006**, *161*, 617–622; c) A. Yoshino, *Angew. Chem. Int. Ed.* **2012**, *51*, 5798–5800.

[10] a) S. Guillot, M. Delsanti, S. Désert, D. Langevin, *Langmuir* **2003**, *19*, 230–237; b) D. Truzzolillo, F. Bordi, C. Cametti, S. Sennato, *Phys. Rev. E* **2009**, *79*, 011804; c) C. G. Lopez, S. E. Rogers, R. H. Colby, P. Graham, J. T. Cabral, *J Polym Sci B Polym Phys* **2015**, *53*, 492–501.

[11] N. M. Wasiuddin, M. M. Zaman, E. A. O'Rear, *Int. J. Pavement Res. Technol.* **2010**, *3*, 1–9.

[12] a) W. Brown, J. Zhao, *Langmuir* **1994**, *10*, 3395–3401; b) A. M. Medeiros, E. Bourgeat-Lami, T. F. McKenna, *Polymer* **2020**, *12*, 1476; c) B. Zeeb, C. Thongkaew, J. Weiss, *J. Appl. Polym. Sci.* **2014**, *131*, 40099.

[13] K. Park, S. Myeong, D. Shin, C. W. Cho, S. C. Kim, T. Song, *J. Ind. Eng. Chem.* **2019**, *71*, 270–276.

[14] a) W. A. Appiah, D. Kim, J. Song, M. H. Ryou, Y. M. Lee, *Batteries & Supercaps* **2019**, *2*, 541–550; b) H. Lee, C. Bak, M. Lim, H. An, S. Byun, Y. M. Lee, H. Lee, *ACS Appl. Nano Mater.* **2023**, *6*, 3128–3137.

[15] W. J. Chang, G. H. Lee, Y. J. Cheon, J. T. Kim, S. I. Lee, J. Kim, M. Kim, W. I. Park, Y. J. Lee, *ACS Appl. Mater. Interfaces* **2019**, *11*, 41330–41337.

[16] H. Han, H. Park, K. C. Kil, Y. Jeon, Y. Ko, C. Lee, M. Kim, C. W. Cho, K. Kim, U. Paik, T. Song, *Electrochim. Acta* **2015**, *166*, 367–371.

[17] W. Choi, H. C. Shin, J. M. Kim, J. Y. Choi, W. S. Yoon, *J. Electrochem. Sci. Technol.* **2020**, *11*, 1–13.

[18] J. Landesfeind, J. Hattendorff, A. Ehrl, W. A. Wall, H. A. Gasteiger, *J. Electrochem. Soc.* **2016**, *163*, A1373.

[19] K. R. Tallman, B. Zhang, L. Wang, S. Yan, K. Thompson, X. Tong, J. Thieme, A. Kiss, A. C. Marschilok, K. J. Takeuchi, D. C. Bock, E. S. Takeuchi, *ACS Appl. Mater. Interfaces* **2019**, *11*, 46864–46874.

[20] D. Billaud, F. Henry, *Solid State Commun.* **2002**, *124*, 299–304.

[21] H. Fujimoto, S. Takagi, K. Shimoda, H. Kiuchi, K.-i. Okazaki, T. Murata, Z. Ogumi, T. Abe, *J. Electrochem. Soc.* **2021**, *168*, 090515.

[22] Z. Chen, D. L. Danilov, L. H. Raijmakers, K. Chayambuka, M. Jiang, L. Zhou, J. Zhou, R.-A. Eichel, P. H. Notten, *J. Power Sources* **2021**, *509*, 230345.

[23] a) H. B. Wu, J. S. Chen, X. W. Lou, H. H. Hng, *J. Phys. Chem. C* **2011**, *115*, 24605–24610; b) Y. Lu, J. Nai, X. W. Lou, *Angew. Chem. Int. Ed.* **2018**, *57*, 2899–2903.

[24] a) X. Chang, W. Li, J. Yang, L. Xu, J. Zheng, X. Li, *J. Mater. Chem. A* **2015**, *3*, 3522–3528; b) N. A. Laziz, J. Abou-Rjeily, A. Darwiche, J. Toufaily, A. Outzourhit, F. Ghamouss, M. T. Sougrati, *J. Electrochem. Sci. Technol.* **2018**, *9*, 320–329.

[25] V. Watson, Y. Yeboah, M. Weatherspoon, J. Zheng, E. E. Kalu, *Int. J. Electrochem. Sci.* **2018**, *13*, 7968–7988.

[26] X. Huang, W. Zhu, J. Yao, L. Bu, X. Li, K. Tian, H. Lu, C. Quan, S. Xu, K. Xu, *J. Mater. Chem. A* **2020**, *8*, 17429–17441.

[27] J. B. Habedank, J. Kriegler, M. F. Zaeh, *J. Electrochem. Soc.* **2019**, *166*, A3940.

[28] A. Missyul, I. Bolshakov, R. Shpanchenko, *Powder Diffr.* **2017**, *32*, S56–S62.

[29] H. Park, J. Kim, D. Lee, J. Park, S. Jo, J. Kim, T. Song, U. Paik, *Adv. Sci.* **2021**, *8*, 2004204.

[30] a) K. N. Wood, G. Teeter, *ACS Appl. Energ. Mater.* **2018**, *1*, 4493–4504; b) D. Lee, S. Sun, C. Kim, J. Kim, K. Park, J. Kwon, D. Song, K. Lee, T. Song, U. Paik, *Appl. Surf. Sci.* **2022**, *572*, 151439.

[31] Z. Xingyu, L. Wang, T. Zhang, K.-h. Lam, *Batteries & Supercaps* **2023**, *6*, e202200495.

[32] L. G. Lu, X. B. Han, J. Q. Li, J. F. Hua, M. G. Ouyang, *J. Power Sources* **2013**, *226*, 272–288.

[33] M. Weiss, R. Ruess, J. Kasnatscheew, Y. Levartovsky, N. R. Levy, P. Minnmann, L. Stolz, T. Waldmann, M. Wohlfahrt-Mehrens, D. Aurbach, *Adv. Energy Mater.* **2021**, *11*, 2101126.

[34] J. Shi, L. Zu, H. Gao, G. Hu, Q. Zhang, *Adv. Funct. Mater.* **2020**, *30*, 2002980.

[35] S. Feiler, P. Daubinger, L. Gold, S. Hartmann, G. A. Giffin, *Batteries & Supercaps* **2023**, *6*, e202200518.

[36] a) K. Xu, A. von Cresce, U. Lee, *Langmuir* **2010**, *26*, 11538–11543; b) N. Ogihara, Y. Itou, T. Sasaki, Y. Takeuchi, *J. Phys. Chem. C* **2015**, *119*, 4612–4619; c) J. Landesfeind, A. Eldiven, H. A. Gasteiger, *J. Electrochem. Soc.* **2018**, *165*, A1122–A1128; d) R. Morasch, J. Landesfeind, B. Suthar, H. A. Gasteiger, *J. Electrochem. Soc.* **2018**, *165*, A3459.

Manuscript received: April 22, 2023
Revised manuscript received: June 12, 2023
Accepted manuscript online: June 27, 2023
Version of record online: July 18, 2023